https://doi.org/10.5194/egusphere-2026-3017
Preprint. Discussion started: 23 June 2026

A segmented-breakpoint sea-surface-temperature upwelling index for the Benguela Upwelling System

Albertus J. Smit[1,2] and Neville Sweijd[3]

[1]Department of Biodiversity and Conservation Biology, University of the Western Cape, Bellville, Cape Town 7535, South Africa
[2]South African Environmental Observation Network, Elwandle Coastal Node, Gqeberha 6031, South Africa
[3]School for Climate Studies, Stellenbosch University, Stellenbosch 7599, South Africa

Correspondence: Albertus J. Smit (ajsmit@uwc.ac.za)

Abstract. Satellite sea-surface-temperature (SST) upwelling indices usually contrast coastal temperature with a fixed offshore reference, although the offshore extent of the surface cool tongue varies across cells and days. We replace the fixed reference with a daily fitted thermal breakpoint from a continuous two-segment regression on cross-shore SST profiles, accepted only when model-evidence, slope-ratio, offshore-baseline, edge-buffer, and residual-autocorrelation criteria are met. We apply the method to five Benguela upwelling cells (UCs) from 2015 to 2025 using two fine-resolution Level-4 SST products, namely the Operational Sea Surface Temperature and Ice Analysis and the Geo-Polar Blended analysis from the US National Oceanic and Atmospheric Administration. Coarser Advanced Very High Resolution Radiometer and microwave optimum interpolation products serve as resolution comparisons. Median fitted breakpoints span 114 to 270 km across UCs, so 50 to 100 km reference points usually sample inside the fitted inshore segment rather than offshore water. In the Operational Sea Surface Temperature and Ice Analysis product, the daily correlation between inshore-segment SST drawdown and the conventional fixed-distance contrast rises from $r = 0.06$ at 50 km to $r = 0.93$ at 500 km, showing that reference distance changes the diagnostic itself. The Lüderitz annual r_{50} point estimate is negative (-0.16), but its block-bootstrap interval includes zero. A paired comparison with a Bakun-type offshore-Ekman-transport flag shows that southern Benguela cells retain SST structure without the local wind flag on ca. one fifth of matched days. The method therefore positions fixed-reference SST indices as structural surface-temperature indicators whose interpretation depends on cell-scale geometry and SST–wind co-activity.

1 Introduction

Upwelling indices (UIs) using satellite-derived sea-surface-temperature (SST) assess the cross-shore contrast between coastal and offshore water to delimit the upwelling-affected zone on a given day and to quantify its surface cooling (Nykjaer and Van Camp, 1994; Santos et al., 2005; Benazzouz et al., 2014a; Vasquez-Cuervo et al., 2013; Seabra et al., 2019). These indices are used across eastern boundary upwelling systems (EBUS) and form the basis of fishery, ecosystem-model, and climate-trend applications that build on the coastal cool-tongue signal. Every published SST-UI implementation fixes the offshore reference distance by convention, sensitivity assessment, or correlation with wind-derived indices (Nykjaer and Van Camp, 1994; Santos et al., 2005; Marcello et al., 2011; Benazzouz et al., 2014a, b), and no formal criterion sets the reference per transect or latitude.

https://doi.org/10.5194/egusphere-2026-3017
Preprint. Discussion started: 23 June 2026

Using SST is one of several approaches for deriving UIs. The closed-isotherm-area and threshold-isotherm indices select an isotherm and report its area or extent, the fixed-distance contrast $UI_{\mathrm{SST}}^{(d_0)} = T_{\mathrm{offshore}} - T_{\mathrm{coast}}$ samples a single offshore reference point at a chosen distance d_0, and the anomaly-event indices count days exceeding a percentile threshold (Marcello et al., 2011; Benazzouz et al., 2014a, b; Abrahams et al., 2021b, a). The closest published data-emergent precedent is the per-latitude-band offshore reference used by Benazzouz et al. (2014a) in the Canary system. Wind-based indices (Bakun, 1973; Chen et al., 2012; Lamont et al., 2018) avoid the SST-reference choice but omit, in their local form, wind-stress-curl pumping, non-local ocean response, and alongshore-advection memory (Benazzouz et al., 2014a; Bordbar et al., 2021; Hutchings et al., 2009), and detect a different phenomenon than the SST-UIs. The shared phenology terminology, namely the number of upwelling days (NUD), the number of upwelling events (NUE), and the total cumulative upwelling magnitude (TCU), is useful, but these quantities compare across studies only after their operational definitions are stated (Bograd et al., 2009; Iles et al., 2012; Lamont et al., 2018; Abrahams et al., 2021b, a).

The fixed-reference assumption has an inferential consequence. Published cross-shore length scales for upwelling-affected water in the Benguela alone span ca. 50–500 km across UC-scale morphometry, curl-driven nearshore bands, and far-field advected footprints (Lutjeharms and Meeuwis, 1987; Bordbar et al., 2021; Pavlushin and Kubryakov, 2022; Brandt et al., 2024; Belonenko et al., 2024), so a single d_0 must sample inside the cool tongue at some UCs and offshore water at others. The magnitude error in $UI_{\mathrm{SST}}^{(d_0)}$ scales with the distance between d_0 and the fitted thermal breakpoint and changes sign across UCs. Production calculations, ecosystem-model coastal boundary conditions, and trend-attribution work that builds on the cross-shore SST contrast therefore inherit a UC-dependent systematic error without a clear justification.

Here we treat the offshore reference as an empirical property of each daily SST profile rather than as a fixed distance imposed before analysis. The resulting breakpoint index, UI_{BR}, asks whether the coastal cool tongue has a detectable inshore–offshore structure and where the fitted thermal breakpoint lies on a given day. It remains an SST-UI, not a wind-forcing index. Like closed-isotherm, threshold-isotherm, fixed-distance, and anomaly-event indices, it describes the surface expression of what one would expect of upwelling-affected water. We use the five major Benguela UCs from Cape Frio to Cape Peninsula as a test case over 2015–2025, then ask three linked questions, namely how far offshore the fitted thermal breakpoint lies, how the resulting SST contrast differs from conventional fixed-distance contrasts, and how often the SST-structure signal agrees with a daily offshore-Ekman wind detector.

With this method, we propose that the breakpoint acceptance flag is an SST structure detector. It does not replace a wind-based UI, and we make no attribution of any single mechanism to SST-structure-only days. We do not validate the breakpoint flag against independent physical predictors (wind-stress curl, alongshore advection proxies, sea-level anomaly, surface heat flux), which in themselves are simply proxies for upwelling and do not provide a direct measure of the physical upwelling process.

https://doi.org/10.5194/egusphere-2026-3017
Preprint. Discussion started: 23 June 2026

2 Methods

2.1 Study area, SST and ancillary inputs

The analysis is restricted to five Benguela UCs, namely Cape Frio, Walvis Bay, Lüderitz, Cape Columbine, and Cape Peninsula (Figure 1). The cross-shore mesh is a curvilinear Laplace-potential streamline construction over the ocean domain bounded by the smoothed Benguela coast and a 500 km coast-distance outer contour. A discrete Laplace equation $\nabla^2\phi = 0$ is solved on a 5 km grid with Dirichlet conditions $\phi = 0$ on a coast band and $\phi = 1$ on a matching band along the outer contour, and the transects of the mesh are the streamlines of ϕ (gradient lines orthogonal to iso-ϕ contours). The streamlines bend smoothly around headlands and are deflected by opposite shores at bay re-entrants, supplemented by short bay-bridge polylines at St Helena Bay (ca. 32.8° S) and False Bay (ca. 34.4° S) so that coastal seeds at the bay mouths project transects into the open ocean rather than into the bay interior. The retained mesh contains 742 transects spaced along the coast from approximately 12° S to 40° S, each sampled at 480 sigma nodes at uniform fractions of arc length along its streamline, and the five UC windows use 189 of these transects. The full construction procedure, including the coastline projection, bathymetric inputs, streamline tracing, and pruning passes that remove crossings and short streamlines, is given in Text S1 in the Supplement. Regression distance x is streamline arc-length, and reported breakpoint positions and reference distances are converted to coast-distance by $x_{\mathrm{coast}} = x \cdot 500/\ell$, where ℓ is the streamline length (Text S1 in the Supplement). The per-(product, day, transect) breakpoint quantities $\{\beta_{\mathrm{in}}, \beta_{\mathrm{off}}, x_b, \widehat{T}_{\mathrm{bg}}\}$ are computed from the four SST products and the mesh described here. SST inputs are Group for High Resolution Sea Surface Temperature (GHRSST) Level-4 (L4) analyses, namely the Operational Sea Surface Temperature and Ice Analysis (OSTIA) and the Geo-Polar Blended analysis from the National Oceanic and Atmospheric Administration (NOAA) Office of Satellite and Product Operations (OSPO) at ca. 0.05° (Worsfold et al., 2024; Maturi et al., 2017), and the Advanced Very High Resolution Radiometer Optimum Interpolation (AVHRR_OI) and Microwave Optimum Interpolation (MW_OI) analyses at ca. 0.25° (Banzon et al., 2016; Wentz and Meissner, 2000). ERA5 10 m winds (Hersbach et al., 2020) support the wind comparison. Adjacent mesh transects are spaced at ca. 4 km, so UC-level aggregates are spatial summaries rather than independent-transect estimates.

2.2 Segmented-breakpoint regression

We fit a continuous two-segment piecewise-linear regression in cross-shore distance x to the SST profile $T_p(x; c, t)$ at every (product, day, transect c):

$$T_p(x;c,t) \;=\; \begin{cases} \alpha_{\mathrm{in}} + \beta_{\mathrm{in}}\, x, & 0 \le x \le x_b \\ \alpha_{\mathrm{in}} + \beta_{\mathrm{in}}\, x_b + \beta_{\mathrm{off}}\,(x - x_b), & x_b < x \le L. \end{cases} \tag{1}$$

The two-segment model has four free parameters $\{\alpha_{\mathrm{in}}, \beta_{\mathrm{in}}, \beta_{\mathrm{off}}, x_b\}$, and the one-segment baseline has two, $\{\alpha, \beta\}$. Continuity at x_b makes the offshore intercept $\alpha_{\mathrm{off}} = \alpha_{\mathrm{in}} + \beta_{\mathrm{in}}\, x_b$ a derived quantity rather than a free parameter. The offshore reference temperature used by the inshore drawdown of Section 2.4 is the mean of the fitted offshore line over $x_b < x \le L$. At each candidate x_b, ordinary least squares (OLS) gives the three slopes / intercepts, and the chosen x_b is the candidate native-pixel

https://doi.org/10.5194/egusphere-2026-3017
Preprint. Discussion started: 23 June 2026

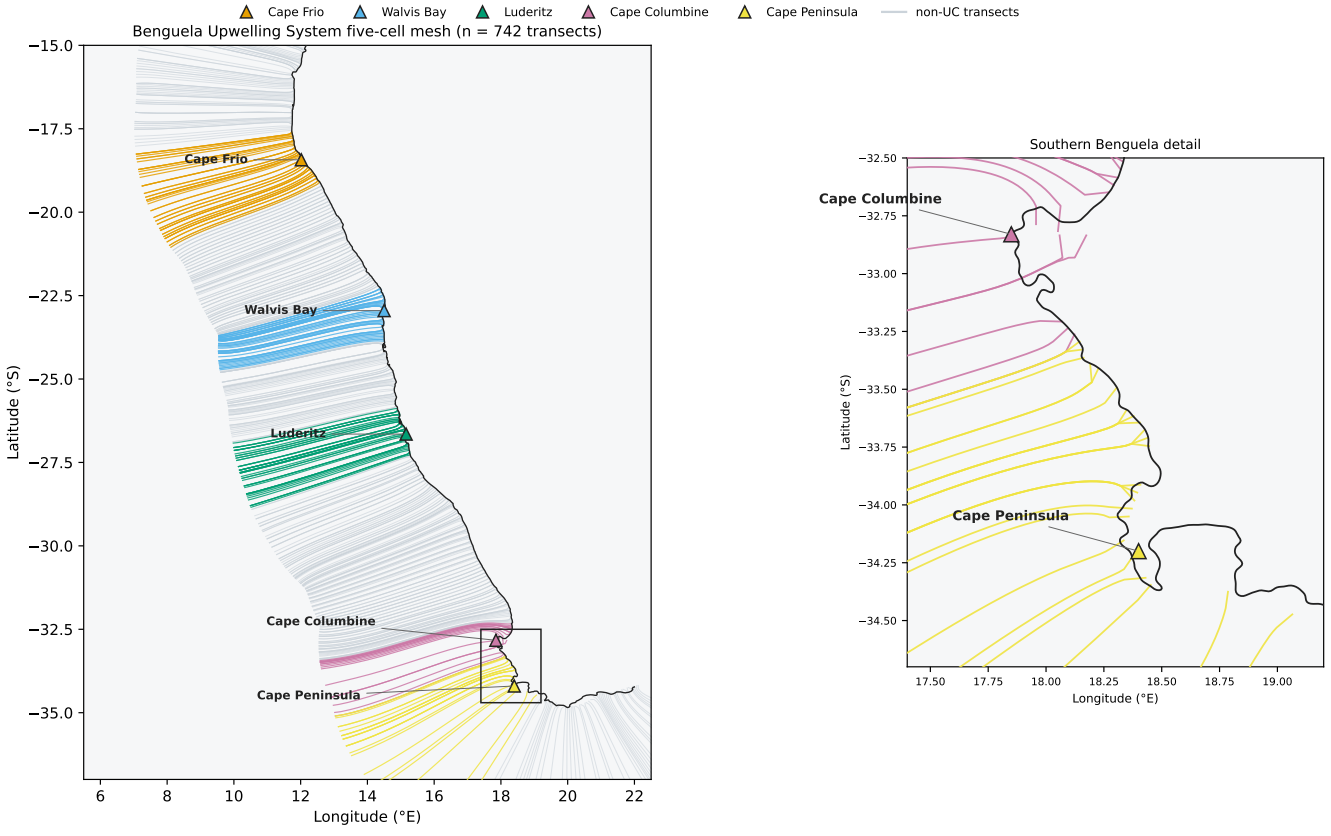

Figure 1. Benguela Upwelling System operational UCs and cross-shore mesh. Grey lines show the retained non-UC transects, and coloured lines show the five UC-window transect sets used in the analysis, with the southern Benguela inset resolving Cape Columbine and Cape Peninsula. UC colours match the other figures.

position that minimises the joint residual sum of squares. We sample one SST observation per native pixel along the transect, so the Akaike information criterion (AIC) evidence uses the product's independent along-profile native-pixel count (median ca. 91–101 in OSTIA / OSPO and ca. 0–23 in AVHRR / MW_OI, with per-(UC, product, season) values in Table S1 in the Supplement). Across-transect pixel uniqueness is then enforced at aggregation, so for each (UC, product, day), each L4 pixel is claimed by the first transect that covers it (first-occurrence-wins on $\mathrm{col\_id}$), and a transect contributes to the per-(UC, product, day) population only if at least one of its pixels survives this deduplication. The within-transect AIC test above is independent of the deduplication, since it uses each transect's own native-pixel sample. We accept at fit when four joint criteria are met. First, $\Delta\mathrm{AIC} = \mathrm{AIC}_{\text{one-seg}} - \mathrm{AIC}_{\text{two-seg}} \geq 4$, namely the "considerably less support" guideline of Burnham and Anderson (2004) for the worse model. Second, the ratio of inshore-to-offshore slope magnitudes is at least 2.0, namely the coastal cooling segment is at least twice as steep as the offshore reference segment. Third, the offshore segment is at least 100 km in streamline arc-length ($\ell - x_b \geq 100$ km), namely a minimum offshore-baseline constraint that regularises the offshore fit by preventing it from being

https://doi.org/10.5194/egusphere-2026-3017
Preprint. Discussion started: 23 June 2026

estimated from a short tail of points. The 100 km value is a regularisation choice, which replaces the fixed offshore reference distance of $UI_{\mathrm{SST}}^{(d_0)}$ with a fitted breakpoint x_b subject to this explicit regularisation. Fourth, the candidate breakpoint is at least an edge-buffer distance from each end of the transect ($x_b \geq 10$ km and $\ell - x_b \geq 10$ km in the grid), excluding breakpoint positions at the immediate coastline or at the outer contour where one segment would be supported by too few points to estimate a slope.

The acceptance threshold values above are baseline choices. We report a threshold-sensitivity assay over each of them, over the across-transect pixel rule, and over the per-UC p_{active} daily-classification threshold, with the tested grid and the per-(UC, product, criterion-value) outcomes given in Table S2 in the Supplement. The outcomes are interpreted as a stability check on the UC descriptions in Section 3.1. The Results sections use the AR(1)-corrected (first-order autoregressive) acceptance set described in the next subsection, and the supporting tables are cited where the corresponding results are introduced.

2.3 Model evidence criteria and effective sample size

The AIC at the stated parameter count fixes the model-evidence bar, but two corrections must be considered when the unique-pixel sample n is small or when residuals are correlated. We report AIC, the small-sample corrected Akaike information criterion (AICc) (Hurvich and Tsai, 1989), and the Bayesian information criterion (BIC) (Schwarz, 1978) side-by-side for the Cape Columbine DJF (December–February) 2020 test subset across all four products (Table S3 in the Supplement). With $n \approx 90$–100 in OSTIA / OSPO, the AICc small-sample correction is negligible (ca. 0.4) and the BIC penalty is about 2.3 times stricter than the AIC penalty per parameter. With $n \approx 19$–23 in AVHRR / MW_OI, the AICc correction rises to ca. 2.2–2.9, still below the $\Delta\mathrm{AIC} \geq 4$ bar. AIC and AICc therefore disagree on only 0.5 % of AVHRR / MW_OI profiles and on 0 % of OSTIA / OSPO profiles in the test subset, with the same disagreement rate for AIC versus BIC. The cross-product positioning of Section 3.1 treats OSTIA and OSPO as primary fine-resolution evidence and AVHRR / MW_OI as coarse-grain diagnostics of product dependence, consistent with the information criterion (IC) sensitivity here and with the AR(1)-corrected acceptance reported below.

Treating the breakpoint x_b as a fourth free parameter alongside the intercept and the two segment slopes ($\{\alpha_{\mathrm{in}}, \beta_{\mathrm{in}}, \beta_{\mathrm{off}}, x_b\}$) is a choice that the standard AIC penalty does not strictly justify, because x_b is selected over a discrete grid rather than estimated within a fixed-grid likelihood. Stricter penalties have been developed for this case, namely the $k \ln n$ BIC-type penalty of Yao (1988) for change-point estimation, the structural-break information criteria of Bai and Perron (1998), and the $(\ln n)^{1+\delta}$ modified-BIC correction of Zhang and Siegmund (2007) for change-point detection on a discrete grid. Rather than assuming a single penalty, we treat this as an IC-sensitivity question, and the AIC, AICc, and BIC agreement (Table S3 in the Supplement) justifies the four-parameter count, because the three criteria return the same accept / reject decision on 100 % of fine-resolution profiles and on 99.5 % of coarse-resolution profiles in the test subset. The few disagreements result from stricter criteria rejecting a marginal coarse-product fit. The IC sensitivity here is separate from the residual-autocorrelation issue addressed in the next paragraph.

We estimate the residual decorrelation length per (UC, season) by fitting an AR(1) to the OLS residuals along the OSTIA 2020 cross-shore unique-pixel sequence of each accepted profile for all UCs and all austral seasons. Lag-1 pairs are pooled

https://doi.org/10.5194/egusphere-2026-3017
Preprint. Discussion started: 23 June 2026

across the accepted profiles in each (UC, season) using only within-profile pairs, so no across-transect autocorrelations influence the estimate. The AR(1) coefficient ϕ ranges 0.884–0.950 with a median of 0.915, so the unique-pixel sample has a strong positive residual autocorrelation after the two-segment fit and the unique-pixel sample size n overestimates the independent-sample information by a large factor. Each ϕ converts to an effective sample size $n_{\text{eff}} = n(1-\phi)/(1+\phi)$ (Chelton, 1983), and we recompute AIC with $n^{\star}_{\text{eff}}$ at every (UC, product, season). The per-(UC, product, season) AR(1)-corrected acceptance is reported in Table S1 in the Supplement and interpreted next to the UC descriptions in Section 3.1. We use the AR(1)-corrected acceptance set for the main climatology, fixed-distance comparison, daily SST-structure classification, paired SST–wind classifier, and block-bootstrap intervals. The baseline $\Delta\text{AIC} \geq 4$ screen is retained only as a profile-shape comparison and as part of the threshold-sensitivity assessment.

2.4 The segmented-breakpoint upwelling index UI_{BR}

The segmented-breakpoint upwelling-structure index UI_{BR} (Section 4.3) is a three-component description of the cross-shore SST profile per (product, day, transect). The first component, the breakpoint position x_b (km), is the data-emergent fitted thermal breakpoint which identifies the offshore extent of the inshore steep-gradient segment on that day at that transect. The second component, the inshore segment slope β_{in} (° C km^{-1}), is the cross-shore rate at which surface SST warms offshore over the inshore segment, and larger $|\beta_{\text{in}}|$ indicates a steeper cross-shore SST gradient near the coast, consistent with stronger upwelling but not exclusive to it. The third component, the inshore SST drawdown $\bar{D}_{\text{in}}$ (° C), is the offshore reference temperature minus the inshore-segment-mean SST:

$$\bar{D}_{\text{in}} = \widehat{T}_{\text{bg}} - \bar{T}_p^{[0,x_b]}, \tag{2}$$

where $\widehat{T}_{\text{bg}}$ is the mean of the fitted offshore segment (Section 2.2) and $\bar{T}_p^{[0,x_b]}$ is the trapezoidal mean of the native-pixel SST values between the coast and the breakpoint. $\bar{D}_{\text{in}}$ is a within-profile contrast, dimensionally and structurally distinct from the fixed-distance contrast $UI_{\text{SST}}^{(d_0)} = T(d_0) - T(0)$ (cool inshore $\rightarrow$ positive, matching the sign of $\bar{D}_{\text{in}}$), and the two should be compared as different estimates of the cross-shore thermal structure rather than as different numerical estimates of the same quantity. Climatological aggregates per (product, season, UC) are the median, the 5th, and the 95th percentile across accepted days at the UC, and inter-annual variability is the analogous per-year aggregate.

2.5 Per-day classification of upwelling-consistent SST structure from the breakpoint acceptance

The AR(1)-corrected breakpoint acceptance flag is the per-day SST-structure detector. A value of 1 means the profile is well described by a steep inshore segment over a gentler offshore segment after the effective-sample correction of Section 2.3. It is not a direct wind-driven-upwelling detector, because a relaxation-day profile can retain the two-segment cool tongue, and a wind-active day can fail the SST-structure test before the surface field responds. At each UC on each day, p_{active} is the fraction of UC-window transects whose breakpoint fit is accepted, and it summarises whether the two-segment cool-tongue signature is spatially coherent across the UC. A day is classified as SST-structure-active when $p_{\text{active}} \geq 0.5$, namely when at least half of the UC's transects show the signature (sensitivity at 0.3 and 0.7 is in Table S4 in the Supplement). Events are sequences of at

https://doi.org/10.5194/egusphere-2026-3017
Preprint. Discussion started: 23 June 2026

least three consecutive SST-structure-active days, with one interior inactive day permitted. The SST-based phenology metrics are $\mathrm{NUD_{BR}}$ (SST-structure days), $\mathrm{NUE_{BR}}$ (SST-structure events), and $\mathrm{TCU_{BR}}$ (cumulative SST-structure magnitude, namely the sum of daily-median $\bar{D}_{\mathrm{in}}$ over SST-structure-active days). These are analogues of wind-based metrics (Lamont et al., 2018) and SST-anomaly event counts (Abrahams et al., 2021b, a). The retained daily-detection and product-specific p_{active} displays are shown in Figs. S1 and S2 in the Supplement. Under the AR(1)-corrected criterion these metrics are reported for OSTIA and OSPO only, and AVHRR and MW_OI are retained in Table S1 in the Supplement as product-resolution references.

2.6 Comparison with other indices

We compare UI_{BR} against two reference groups, namely the fixed-distance SST contrasts and a wind-based index. The fixed-distance group is the conventional SST contrast $UI_{\mathrm{SST}}^{(d_0)} = T(d_0) - T(0)$ in the cool-coastal-positive sign convention (so positive values match the sign of $\bar{D}_{\mathrm{in}}$), computed at $d_0 \in \{50, 100, 200, 500\}$ km. These four distances span the curl-driven nearshore band, Benguela UC-scale SST extents, and the far-field advected footprint of upwelled water (Lutjeharms and Meeuwis, 1987; Bordbar et al., 2021; Pavlushin and Kubryakov, 2022; Brandt et al., 2024; Belonenko et al., 2024). The fixed-distance contrast $UI_{\mathrm{SST}}^{(d_0)}$ and the data-emergent contrast $\bar{D}_{\mathrm{in}}$ are different estimands of the cross-shore thermal structure, namely a point contrast at d_0 versus a segment mean over the inshore segment, and the Pearson r between them is informative about co-variability but is not a calibration. We denote by r_{d_0} the daily Pearson correlation between $\bar{D}_{\mathrm{in}}$ and $UI_{\mathrm{SST}}^{(d_0)}$ aggregated over all accepted days of the operational window, with r_{50} as the value at $d_0 = 50$ km. We add a like-for-like geometric statistic, $P(d_0 < x_b)$ per UC, season, product, and threshold setting, with block-bootstrap intervals.

The wind-based group has two separate constructs that should not be conflated. The continuous Bakun offshore Ekman-transport index UI_w (Bakun, 1973), computed from ERA5 daily-mean 10 m winds, is aggregated to July–June TCU on the 2015–2025 window and used for the $\mathrm{TCU_{BR}}$–TCU_w correspondence comparison. The daily binary wind detector, which informs the paired classifier of Section 2.7 and the NUD / NUE comparison, is akin to the Bakun offshore-Ekman-transport detector, so it flags a day at a UC as wind-active when the daily-mean Bakun offshore Ekman transport at the UC is positive ($UI_w > 0$), namely when the alongshore-equatorward wind component, rotated to the local coast-normal direction following Lamont et al. (2018), drives net offshore Ekman transport in the southern-hemisphere upwelling-favourable sense. The daily-aggregation rule averages hourly ERA5 winds to a single daily value, and events are linked across at most one interior non-favourable day. This is not the full Lamont et al. (2018) event threshold, because it uses the sign of offshore transport rather than a local wind-speed threshold. Annual $\mathrm{TCU_{BR}}$ correlations use product-UC-years when available.

2.7 Paired-classifier diagnostic

The SST-structure detector and the Bakun-analogous wind detector (Section 2.6) are two independent classifiers of the daily state, neither of which is the truth. Per (UC, product, season), we report six agreement statistics on the matched pair, namely balanced accuracy (the mean of sensitivity and specificity, treating each detector's active flag as the positive class), sensitivity (taking the wind detector as the reference for the breakpoint detector and vice versa), specificity (the same, complementary), Matthews correlation coefficient (MCC) (Matthews, 1975), raw agreement p_o, and Cohen's κ. MCC is the summary statistic at

https://doi.org/10.5194/egusphere-2026-3017
Preprint. Discussion started: 23 June 2026

perennial-wind UCs where Cohen's κ is compressed by saturated marginals (Byrt et al., 1993; Chicco and Jurman, 2020). We present the κ–wind-marginal diagnostic in Fig. S3 in the Supplement.

To construct the paired classifier (concordant active, concordant quiet, SST-structure-only, wind-only), we create a date-shuffled-within-season null baseline. For each (UC, product, season), we permute the breakpoint detector's daily flags within season, recompute every paired-classifier statistic, repeat 1000 times, and report the 95 % interval of the shuffled distribution alongside the observed statistic (Table S5 in the Supplement). The null tests whether the observed agreement exceeds chance at the within-season scale, but it does not test mechanism.

2.8 Uncertainty

We calculate block-bootstrap 95 % intervals for the main statistics. Alongshore blocks are constructed at the UC scale with two block sizes, 25 km and 50 km. Year and season are resampled in blocks where the aggregated metric is annual or seasonal, and cross-product comparisons resample products in pairs to preserve the day-level matching. The reported intervals are 1000-replicate bootstrap percentile intervals.

The block bootstrap above describes uncertainty around UC-scale summaries (e.g. the median x_b per UC, the sBUS SST-structure-only fraction), and it is not, on its own, a statement about identifiability of an individual breakpoint. We therefore report per-profile x_b uncertainty on a stratified random sample of the 2020 accepted set, so per (UC, product, season) using OSTIA and OSPO, we draw 100 accepted profiles (4000 profiles in total), and for each we resample the unique-pixel sample $(x, T_p(x))$ with replacement 1000 times, rerun the candidate-breakpoint grid search at each resample, and record the resulting $\hat{x}_b^\star$. The per-profile 95 % bootstrap interval reports identifiability of the breakpoint for that individual profile, and a bimodal test (Gaussian kernel density estimate, KDE, peaks at prominence $\geq 0.1 \max$ separated by more than 50 km) flags profiles whose objective function admits a secondary inflexion. Per-(UC, product) summaries of the confidence interval (CI) width distribution and the bimodal-flag rate are in Table S6 in the Supplement, and per-UC empirical cumulative distribution functions (CDFs) of CI width are in Fig. S4 in the Supplement.

3 Results

3.1 UC characterisation across four products

Our main findings are based in OSTIA and OSPO, the two fine-resolution L4 analyses that retain usable inshore SST at every UC and retain substantial accepted-profile populations after AR(1) residual decorrelation. After AR(1)-correction (Methods Section 2.3), OSTIA and OSPO lose a median 24 % and 20 % of baseline acceptance respectively across the (UC, season) combinations, with the per-(UC, product, season) pre- and post-correction p_{active} (Table S1 in the Supplement). AVHRR and MW_OI retain no accepted profiles at any (UC, season), so they offer only product-resolution insight rather than breakpoint estimates. OSTIA and OSPO reveal UC-specific breakpoint signatures (Table 1). The annual median offshore extent x_b spans 114–270 km across the five UCs, namely 114 km at Cape Peninsula, 153–159 km at Cape Frio, 156–159 km at Lüderitz, 175–

https://doi.org/10.5194/egusphere-2026-3017
Preprint. Discussion started: 23 June 2026

181 km at Cape Columbine, and 264–270 km at Walvis Bay. Per-(UC, product) annual medians of the inshore SST drawdown $\bar{D}_{\mathrm{in}}$ range 2.05–3.21 °C, with the lower bound at Cape Frio with OSPO and the upper bound at Lüderitz seen in OSTIA. The per-(UC, product, season) breakdown of x_b, $\bar{D}_{\mathrm{in}}$, β_{in}, and the four fixed-distance contrasts $UI_{\mathrm{SST}}^{(d_0)}$ is in Table S7 in the Supplement for the austral-season modulation underlying the annual medians.

Table 1. Climatological annual medians of UI_{BR} components per UC and fine-resolution product, computed on the AR(1)-corrected accepted-profile set and averaged over the four austral seasons across 2015–2025. AVHRR and MW_OI are excluded from the primary table because the AR(1)-corrected acceptance criterion returns no accepted coarse-product profiles in the UC-season tests (Table S1 in the Supplement). $\bar{D}_{\mathrm{in}}$ is in °C; x_b is in km coast-distance; β_{in} is in °C km^{-1}.

UC	Product	$\bar{D}_{\mathrm{in}}$ (°C)	x_b (km)	β_{in} (°C km^{-1})
Cape Frio	OSTIA	2.08	153	0.021
	OSPO	2.05	159	0.020
Walvis Bay	OSTIA	2.54	264	0.017
	OSPO	2.43	270	0.015
Lüderitz	OSTIA	3.21	156	0.034
	OSPO	3.16	159	0.032
Cape Columbine	OSTIA	2.55	175	0.030
	OSPO	2.41	181	0.027
Cape Peninsula	OSTIA	2.53	114	0.043
	OSPO	2.16	114	0.042

Per-profile x_b identifiability, namely the width of the bootstrap interval on an individual accepted fit, is distinct from the UC-median summaries. On the stratified random sample of 4000 accepted 2020 profiles (Section 2.8; Table S6 in the Supplement and Fig. S4 in the Supplement), the per-profile 95 % bootstrap CI on $\hat{x}_b$ has a median width of 22.5 km pooled across the five UCs, 90.8 % of profiles have widths below 100 km, and 5.4 % are flagged bimodal. The median CI width is comparable across the five UCs (21.5–27.4 km per UC), and OSPO has systematically narrower per-profile intervals than OSTIA on the same (UC, season) combinations (median 17–23 km in OSPO versus 22–28 km in OSTIA). Bimodality fractions range 0.03–0.08 per UC. The per-profile breakpoint is therefore well-identified on the typical accepted profile across all five UCs, with a small tail of profiles ($\sim$ 5–10 %) whose objective function has either a wide CI or a secondary inflexion. The UC-median summaries below do not transfer per-profile uncertainty, but the assessment supports their interpretation as UC-scale point estimates rather than averages over widely-uncertain individual fits.

A rejected profile is one that fails the joint ΔAIC, slope-ratio, offshore-segment-length, and edge-buffer criteria of Section 2.2, namely a profile with no detectable two-segment cool-tongue signature, and we interpret a rejection as evidence that the SST field does not have a two-segment cross-shore structure consistent with coastal upwelling on that day at that transect.

https://doi.org/10.5194/egusphere-2026-3017
Preprint. Discussion started: 23 June 2026

The per-(day, transect) rejection rate in the OSTIA representative-profile population (Fig. S5 in the Supplement) varies by more than an order of magnitude across the five UCs. Pooled across DJF and JJA (June–August), rejection is 8.9 % at Cape Frio, 30.5 % at Walvis Bay, 0.7 % at Lüderitz, 3.5 % at Cape Columbine, and 23.4 % at Cape Peninsula. Walvis Bay's season rejection rate is the highest of the five and coincides with its largest accepted x_b (259 km in the DJF–JJA OSTIA population) and shallowest accepted β_{in} ($+0.014\,^\circ\,\text{C}\,\text{km}^{-1}$). The per-season rejected profiles at four of the five UCs still have a gradual cross-shore gradient (ca. $+0.004$ to $+0.011\,^\circ\,\text{C}\,\text{km}^{-1}$ when DJF and JJA are pooled), so the rejection criterion mostly screens monotonic-without-inflexion profiles rather than flat profiles. Cape Peninsula is the exception, with near-zero rejected slopes (pooled ca. $+0.001\,^\circ\,\text{C}\,\text{km}^{-1}$), namely a thermally featureless cross-shore field with neither the upwelling signature nor any background cross-shore gradient.

The UC descriptions above use the baseline acceptance thresholds of Section 2.2, and the threshold-sensitivity assay (Table S2 in the Supplement) shows that they are insensitive to those choices. All five OSTIA UCs continue to satisfy $P(x_b > 50\,\text{km}) \geq 0.5$ at every tested value of every threshold, so our claim that conventional 50 km references sit inside the fitted inshore segment does not depend on the baseline thresholds. The Lüderitz annual r_{50} keeps a negative sign in OSTIA across the grid (-0.16 to -0.14) and supports the negativity claim (see Section 3.2). Per-(UC, product) acceptance fractions are most sensitive to the offshore-baseline criterion, so at 200 km, Walvis Bay OSTIA / OSPO acceptance falls from 0.77 to 0.52 / 0.48 (33 / 36 % relative loss), while the other four UCs lose at most 6 % on the fine-resolution products. The 100 km baseline is therefore the compromise between offshore-baseline length and accepted-profile coverage at the broader UCs.

3.2 Breakpoint position and fixed-distance comparison

Figure 2 compares UI_{BR} ($\bar{D}_{\text{in}}$) against $UI_{\text{SST}}^{(d_0)}$ at 50, 100, 200, and 500 km in the AR(1)-corrected OSTIA set. Pooled across UCs, the correlation is strongest at $d_0 = 500$ km ($r = 0.93$) and decreases as d_0 moves inshore, with $r = 0.79$, 0.44, and 0.06 at 200, 100, and 50 km respectively (Table S8 in the Supplement). Figure 3 shows the underlying pattern. At 50–100 km the breakpoint usually lies offshore of the reference distance, so the reference point is still inside the cool tongue. At 200 km the result is UC-dependent, and in OSTIA, $P(x_b \leq 200\,\text{km})$ spans 0.32 at Walvis Bay to 0.98 at Cape Peninsula. Only 500 km is offshore of the breakpoint at every UC in OSTIA and OSPO.

At the most pronounced year-round UC in the primary fine-resolution products, the daily Pearson correlation between $\bar{D}_{\text{in}}$ and $UI_{\text{SST}}^{(50)}$ is negative in the annual aggregate but not consistently negative across individual seasons (Table S8 in the Supplement). We use Lüderitz in OSTIA as the exemplar case because it has the strongest annual median $\bar{D}_{\text{in}}$ across the five UCs (Section 3.1) and OSTIA is the primary fine-resolution product. The annual aggregate r_{50} at Lüderitz in OSTIA is -0.16 with an alongshore 50 km block-bootstrap 95 % interval of $[-0.21, +0.13]$ (Table S9 in the Supplement), namely the annual sign-inversion holds in point estimate but the interval encompasses zero. The same UC at $d_0 = 500$ km gives $r = 0.93$ in the annual aggregate. The seasonal r_{50} tests are Benjamini–Hochberg adjusted to control the false discovery rate (FDR) across the 40 UC-product-season tests. The FDR-controlled negative cases occur at Cape Peninsula in MAM (March–May) in OSTIA ($r_{50} = -0.19$, $q < 0.0001$) and OSPO ($r_{50} = -0.22$, $q < 0.0001$), at Lüderitz in MAM in OSPO ($r_{50} = -0.16$, $q < 0.0001$), and at Walvis Bay in SON (September–November) in OSPO ($r_{50} = -0.13$, $q < 0.001$). Cape Frio does not support a negative

https://doi.org/10.5194/egusphere-2026-3017
Preprint. Discussion started: 23 June 2026

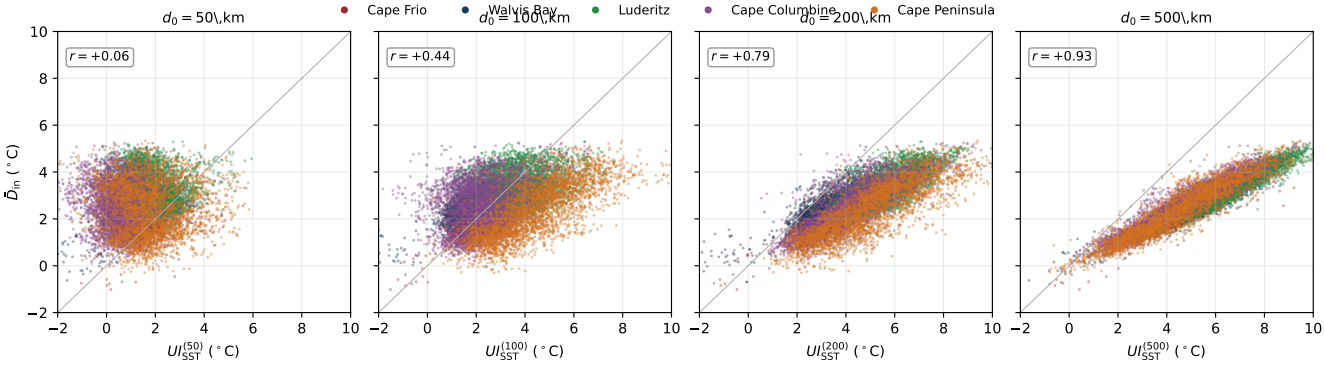

Figure 2. OSTIA daily intensity of UI_{BR} on the AR(1)-corrected accepted set (inshore SST drawdown $\bar{D}_{\mathrm{in}}$, daily median across UC-window transects, y-axis, expressed in °C) against the fixed-distance contrast $UI_{\mathrm{SST}}^{(d_0)} = T_{\mathrm{offshore}} - T_{\mathrm{coast}}$ (x-axis, expressed in °C) at four reference distances: $d_0 = 50, 100, 200, 500$ km, one per panel. The five UCs are colour-coded, and the grey line is the 1:1 reference. Pearson r is annotated in each panel, and the full AR(1)-corrected per-(UC, product, season) d_0 correlation table is in Table S8 in the Supplement.

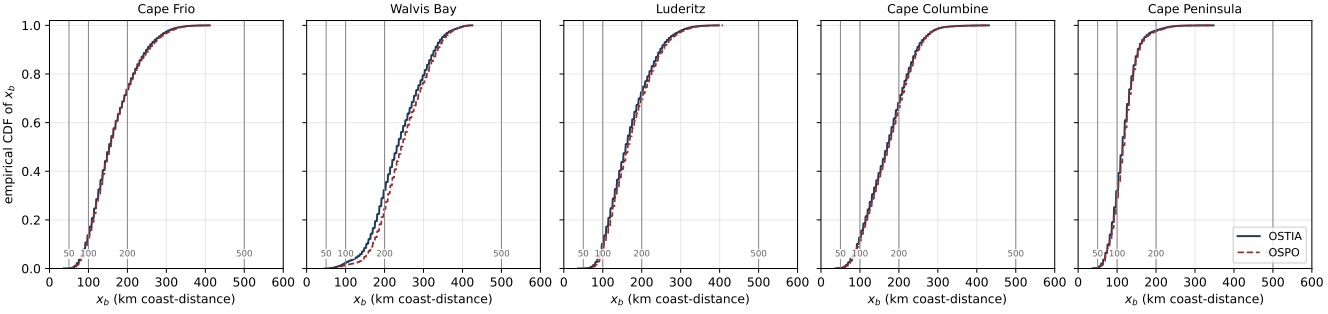

Figure 3. Empirical cumulative distribution of the data-emergent breakpoint position x_b at each UC across the 11-year analysis window on the AR(1)-corrected accepted set, reported in km coast-distance via the linear streamline-stretch approximation of Methods Section 2.1. Five panels arranged horizontally (one per UC) show the per-product empirical CDFs as line styles: OSTIA solid and OSPO dashed. Vertical grey lines mark the four reference distances $d_0 = 50, 100, 200, 500$ km used in the present analysis.

seasonal claim in the AR(1)-corrected accepted dataset. When r_{50} is negative, days on which $UI_{\mathrm{SST}}^{(50)}$ reports stronger contrast coincide with days on which $\bar{D}_{\mathrm{in}}$ weakens.

3.3 Per-day SST-structure classification and the SST–wind agreement

The AR(1)-corrected acceptance flag, aggregated to a per-UC daily activity fraction p_{active}, gives a per-day binary structure classification in OSTIA and OSPO. Lüderitz and Cape Columbine remain near year-round SST-structure-active UCs, i.e. annual $\mathrm{NUD}_{\mathrm{BR}}$ medians are 339 / 330 days at Lüderitz and 332 / 322 days at Cape Columbine in OSTIA / OSPO respectively (Table S10 in the Supplement). Cape Frio is intermediate, with annual $\mathrm{NUD}_{\mathrm{BR}}$ medians of 221 / 228 days. Walvis Bay is the

https://doi.org/10.5194/egusphere-2026-3017
Preprint. Discussion started: 23 June 2026

strict-criterion edge case, with annual medians of 118 / 117 days and several years whose annual median p_{active} is near zero. Cape Peninsula has pronounced austral-summer p_{active} maxima alternating with winter relaxations.

Paired SST–wind daily-classifications are in Figure 4. Each matched UC–product–day is classified by the SST-structure detector and the wind detector, producing four joint classes, namely concordant SST-structure-active (both agree on an active day), concordant quiet (both agree on a quiet day), SST-structure-only (structure-positive but no wind-active flag), and wind-only (wind-active but no breakpoint acceptance). Lüderitz is concordant-active dominated in OSTIA / OSPO (mean seasonal fraction 0.83 on both products), while Walvis Bay becomes wind-only dominated under the strict criterion in MAM and JJA (Table S5 in the Supplement). At southern Benguela Upwelling System (sBUS) UCs, SST-structure-only days account for a mean 0.23–0.24 of matched days at Cape Columbine and 0.17–0.19 at Cape Peninsula in OSTIA / OSPO. The sBUS-pooled fraction is 0.20–0.21 with alongshore 25–50 km block-bootstrap 95 % intervals of ca. 0.16–0.22 (Table S9 in the Supplement). We reiterate that these fractions are descriptive classification outcomes, and they do not identify the physical mechanism of the SST-structure-only days.

4 Discussion

The segmented-breakpoint regression gives a per-day, per-transect fitted thermal breakpoint that varies systematically across the Benguela UCs and that, at most UCs, lies offshore of the conventional 50–100 km fixed references. We discuss this finding around three points. First, the UC-dependent breakpoint position means that no single d_0 matches every UC. Second, the daily Pearson correlation between $\bar{D}_{\mathrm{in}}$ and $UI_{\mathrm{SST}}^{(50)}$ can be weak or negative under the AR(1)-corrected accepted set, with the Lüderitz annual point estimate negative but not significant by block bootstrap. Third, the paired SST–wind classification gives a four-class daily decomposition with SST-structure-only fractions near one fifth at the southern Benguela UCs, which we note but do not attribute.

4.1 Conventional fixed-distance references mis-position the fitted thermal reference

The data-emergent SST-UI literature has two dominant approaches. The per-latitude-band offshore reference of Benazzouz et al. (2014a) replaces a globally fixed d_0 with a regionally fitted one along the Canary system, and the subsequent two-dimensional image-segmentation approaches (Belmajdoub et al., 2024) delineate the areal upwelling footprint in the SST field directly rather than along a one-dimensional transect. Our method belongs to a related one-dimensional approach that fits a cross-shore thermal breakpoint and associated inshore drawdown along a transect mesh per (day, transect), preserving the cross-shore profile interpretation of the existing SST-based UIs while removing its fixed-distance assumption. Two-dimensional segmentation maps the areal footprint, and our one-dimensional method estimates a per-profile breakpoint and an integrated drawdown intensity. The two approaches answer different questions, and an EBUS-scale synthesis would benefit from running them in parallel rather than treating either as a replacement.

Like other eastern boundary upwelling systems, the Benguela has no single literature-standard offshore reference distance for SST-based upwelling indices. Published length scales span ca. 100–380 km across UCs in Lutjeharms and Meeuwis (1987),

https://doi.org/10.5194/egusphere-2026-3017
Preprint. Discussion started: 23 June 2026

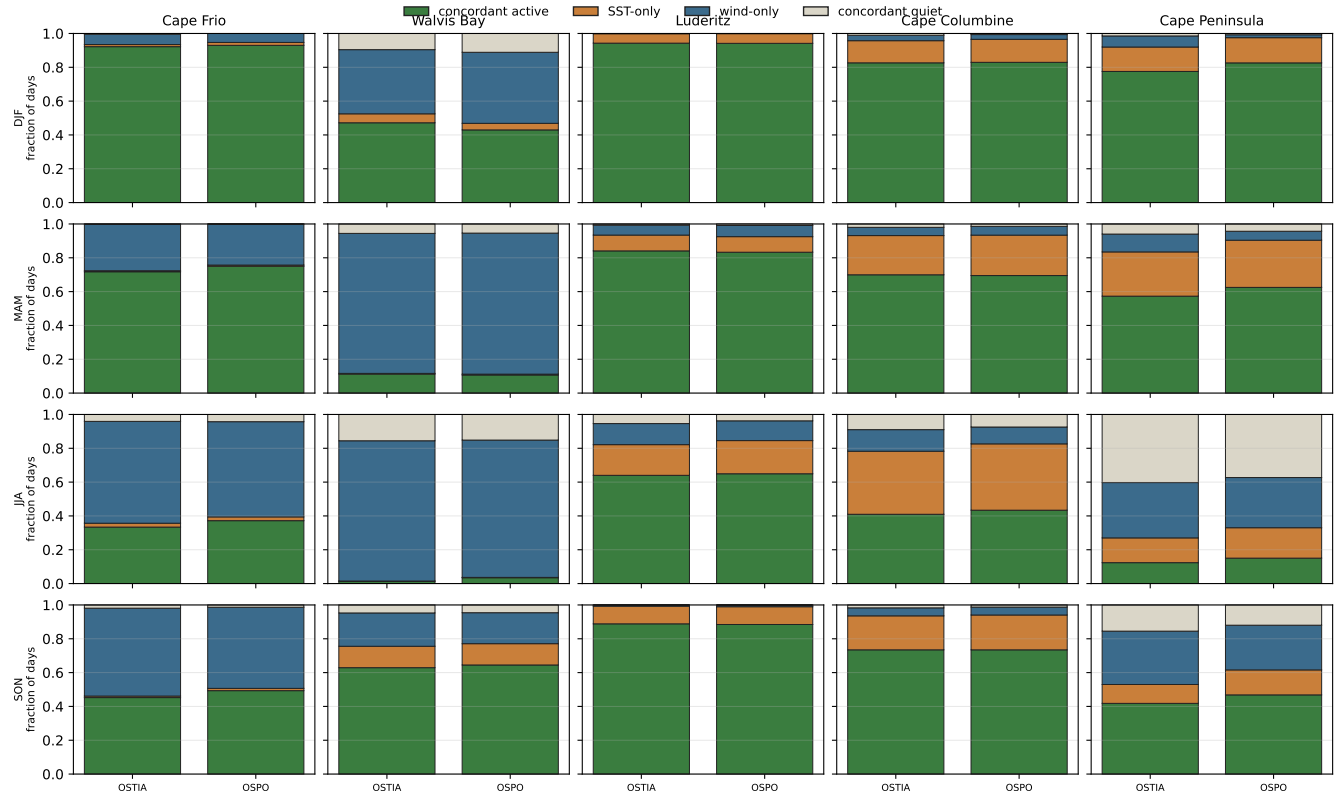

Figure 4. Per-(UC, product, season) four-class decomposition of daily SST–wind classification on the AR(1)-corrected OSTIA and OSPO accepted set, shown as a season-by-UC grid with product bars within each panel. SST-active = $p_{\mathrm{active}} \geq 0.5$ (Methods Section 2.5), and wind-active = daily-mean Bakun offshore Ekman transport at the UC positive, $UI_w > 0$, where UI_w is computed from ERA5 10 m winds rotated to the local equatorward unit vector following the convention of Lamont et al. (2018) (Methods Section 2.6). The four classes are concordant SST-structure-active (both detectors flag the day), concordant quiet (neither does), SST-structure-only, and wind-only.

315 70–250 km in later SST morphometric work (Pavlushin and Kubryakov, 2022; Brandt et al., 2024), 50–150 km for wind-stress-curl-driven upwelling (Bordbar et al., 2021), and advected footprints up to ca. 300–500 km in eddy-resolving tracking (Belonenko et al., 2024). A single fixed reference will therefore lie inshore of the breakpoint at some UCs and offshore at others, so any conventional $UI_{\mathrm{SST}}^{(d_0)}$ will over- or under-estimate the fitted cool-tongue contrast at all but a coincidentally matching UC. For applications that build on this estimate, namely fishery production-potential calculations and ecosystem-model coastal-
320 boundary conditions, the resulting magnitude error scales with the cross-shore distance between the fixed reference and the fitted breakpoint, and it changes sign across UCs.

The median fine-product breakpoint position, 114–270 km across the five UCs (Section 3.1, Table 1, and Figure 1), overlaps Benguela UC-scale and curl-driven reference bands but lies inshore of the far-field advected-footprint scale. The strong agreement between $\bar{D}_{\mathrm{in}}$ and $UI_{\mathrm{SST}}^{(500)}$ in OSTIA pooled across UCs ($r = 0.93$ in Section 3.2) is therefore a benchmark between

https://doi.org/10.5194/egusphere-2026-3017
Preprint. Discussion started: 23 June 2026

related indices, not proof that a 500 km fixed point is mechanistically preferable, since $\bar{D}_{\mathrm{in}}$ averages over a per-day inshore segment whereas $UI_{\mathrm{SST}}^{(d_0)}$ samples one fixed offshore point. A user applying $UI_{\mathrm{SST}}^{(50)}$ at Lüderitz, Cape Peninsula, or Walvis Bay is therefore tracking a signal whose seasonal correlation with the inshore-drawdown interpretation of UI_{BR} can change sign across season, product, and UC (Section 3.2). The sign reversal arises because the 50 km reference point sits inside the fitted inshore segment, so as the segment extends offshore of 50 km, the contrast measured by $UI_{\mathrm{SST}}^{(50)}$ reverses relative to the integrated drawdown $\bar{D}_{\mathrm{in}}$. The sensitivity to the offshore-baseline distance is most pronounced at Walvis Bay, where the 200 km criterion costs 33–36 % of acceptance (Section 3.1). This loss, together with the UC's high rejection rate and shallow accepted β_{in}, is consistent with the broader and more diffuse cool-tongue configuration described for this UC by Hutchings et al. (2009) and Lutjeharms and Meeuwis (1987).

4.2 SST-structure-only days at the southern Benguela UCs

The four-class decomposition has a direct application consequence at the sBUS UCs. An SST-only index reports continued SST-structure-active conditions at Cape Columbine and Cape Peninsula across ca. one fifth of days that the Bakun-positive wind detector reports as quiet (Section 3.3), and the two detectors therefore diverge most at the UCs where the surface signature persists without local wind activity. Candidate mechanisms include wind-stress-curl pumping (Bordbar et al., 2021), alongshore advection from upstream UCs (Hutchings et al., 2009; Benazzouz et al., 2014a), mesoscale retention, non-local ocean response to remote forcing (Benazzouz et al., 2014a), and timing mismatch between sub-daily wind variability and daily-mean Level-4 SST. We list these as plausible explanations, but we do not diagnose their relative contributions. UC-specific behaviours reinforce the four-class structure. Walvis Bay's low $\mathrm{NUD}_{\mathrm{BR}}$ is consistent with its broader cool-tongue configuration, which depresses the per-profile acceptance rate under the strict criterion. Cape Peninsula's pronounced austral-summer p_{active} maxima alternating with winter relaxations reflect the stop-start pulsed-upwelling regime characteristic of the southern Benguela, where favourable-wind days are partitioned into more, shorter events than in the northern Benguela Upwelling System (nBUS) (Lamont et al., 2018; Hutchings et al., 2009; Kämpf and Chapman, 2016). The thermally featureless rejected profiles at Cape Peninsula (near-zero cross-shore gradient) are the surface expression of full wind relaxation and surface warming at the southernmost UC.

4.3 Proxy status and a structural-terminology recommendation

The breakpoint index UI_{BR} developed here, the fixed-distance contrast $UI_{\mathrm{SST}}^{(d_0)}$ used as its benchmark, the closed-isotherm-area indices of Lutjeharms and Meeuwis (1987) and Hagen et al. (2001), the SST-gradient indices of Benazzouz et al. (2014a) and Vasquez-Cuervo et al. (2013), the anomaly-event indices of Abrahams et al. (2021b, a), and the Bakun offshore-Ekman-transport index UI_w of Bakun (1973) and Lamont et al. (2018) all detect a feature of the surface SST field or of the surface wind field that is consistent with the action of coastal upwelling. None of these indices has been validated, at the per-(UC, day, transect) level used by the present paper, against independent measurements of vertical velocity, against the South Atlantic Central Water (SACW) hydrographic signature (Lutjeharms and Valentine, 1987; Lamont et al., 2015), against sea-level anomaly, against wind-stress curl, or against the surface heat budget. The validation gap is field-wide and pre-dates the break-

https://doi.org/10.5194/egusphere-2026-3017
Preprint. Discussion started: 23 June 2026

point formulation. The convention of calling any of these objects an "upwelling index" is inherited from the early SST-UI literature rather than earned by per-product physical validation, and the proxy positioning therefore applies to every member of this kind of UI rather than to the breakpoint formulation in particular.

We therefore use *upwelling-structure metric* (USM) as a cautious descriptor for UIs, namely structural descriptors of features in the surface SST or surface-wind field that are consistent with the action of coastal upwelling without implicating the physical mechanism. Under this definition, the breakpoint x_b identifies a *fitted thermal breakpoint* in the cross-shore SST profile; the inshore drawdown $\bar{D}_{\mathrm{in}}$ is a *within-profile thermal contrast* against the fitted offshore baseline; $UI_{\mathrm{SST}}^{(d_0)}$ records a *fixed-distance thermal contrast*; the closed-isotherm-area indices delineate a *closed-isotherm SST region*; the anomaly-event indices record a *cool-anomaly event*; and the wind index UI_w records a *wind-driven Ekman-transport-favourable state* at the coast. None of these names asserts that the detected object is the physical edge or the physical event of upwelled water at the surface. Each names the structural feature the detector responds to. We retain the UI notation throughout the paper to remain compatible with the existing literature, but the positioning here is the structural one.

4.4 Limitations and forward look

The five-UC selection is operational, namely the high-signal Benguela UCs where the breakpoint regression accepts profiles persistently on the fine-resolution products. We do not yet test weaker or transitional sectors such as Namaqualand, north of Cape Frio, or the Agulhas-influenced coast south of Cape Peninsula. AVHRR and MW_OI are useful for documenting product-resolution sensitivity, but they are not used for inference because the AR(1)-corrected acceptance criterion gives zero accepted coarse-product profiles in the tested UC-season combinations.

Bathymetric controls on x_b, namely whether the data-emergent breakpoint co-locates with the shelf break or with another bathymetric feature, are outside the scope of the present analysis. A shelf-break comparison would require deriving shelf-break distance along the same operational transect mesh.

UI_{BR} can replace a fixed offshore-reference threshold with explicit statistical and operational thresholds, but it does not remove thresholds. A self-contained assay over $p_{\mathrm{active}} \in \{0.3, 0.5, 0.7\}$ keeps the broad OSTIA / OSPO $\mathrm{NUD}_{\mathrm{BR}}$ ranking, namely Lüderitz and Cape Columbine remain near year-round active, Walvis Bay remains the lowest-NUD fine-product UC, and Cape Peninsula is the most threshold-sensitive southern UC (Table S4 in the Supplement). The same definitional caution applies to wind-derived NUD, SST-anomaly signals, weekly frequency-of-occurrence, and $\mathrm{NUD}_{\mathrm{BR}}$.

5 Conclusions

First, a daily two-segment regression applied to cross-shore SST profiles gives a data-emergent fitted thermal breakpoint x_b, an inshore-drawdown intensity $\bar{D}_{\mathrm{in}}$, and an AR(1)-corrected acceptance flag that serves as a per-day SST-structure detector. In the five Benguela UCs across 2015–2025, median x_b on fine-resolution products spans 114–270 km, so the conventional 50–100 km fixed offshore references sample inside the fitted inshore segment on most accepted profiles.

https://doi.org/10.5194/egusphere-2026-3017
Preprint. Discussion started: 23 June 2026

Second, the choice of reference distance can reverse or weaken the diagnostic. At Lüderitz, the annual aggregate point estimate is negative ($r_{50} = -0.16$, block-bootstrap 95 % interval $[-0.21, +0.13]$) but the interval encompasses zero. FDR-controlled negative seasonal r_{50} values occur in Cape Peninsula MAM on both fine products and in Lüderitz MAM and Walvis Bay SON in OSPO. Only the 500 km reference sits past the breakpoint at every UC, so its agreement with $\bar{D}_{\mathrm{in}}$ is benchmarking between related indices rather than evidence that 500 km is the correct fixed reference.

Third, the paired SST–wind classification gives a four-class daily decomposition rather than a binary one, and SST-structure-only days account for ca. one fifth of matched days at the southern Benguela UCs in OSTIA / OSPO. Users such as fishery scientists, ecosystem-modellers, and trend-attribution researchers who build on the cross-shore SST contrast should expect rescaling of UC-level magnitudes and gain the four-class classification of SST–wind co-activity. Our 2015–2025 window is not used to estimate trends.

Fourth, the breakpoint x_b, the inshore drawdown $\bar{D}_{\mathrm{in}}$, and the per-day SST-structure detector identify features of the SST field that are consistent with coastal upwelling without independently establishing the physical mechanism, and the same caveat applies to the fixed-distance, closed-isotherm, anomaly-event, and Bakun-wind indices that the paper benchmarks against. We therefore use the umbrella term *upwelling-structure metric* for the group of UIs (Section 4.3) and treat independent physical validation against hydrography, current, sea-level, wind-stress-curl, or heat-flux evidence as a separate empirical task.

The practical consequence is that a Benguela SST upwelling index must state its offshore reference, spatial scale, and wind relationship before its values are compared across cells or years. A 50 km contrast, a 500 km contrast, and a fitted inshore drawdown describe different parts of the surface thermal field. Substituting one for another changes the inferred UC ranking, event persistence, and SST–wind co-activity. The breakpoint approach makes that dependence visible, so applications in fisheries, ecosystem modelling, and climate attribution can distinguish a change in surface thermal structure from a change introduced by the index definition.

Code and data availability. The four operational SST products, namely OSTIA, OSPO Geo-Polar Blended, AVHRR OI, and MW OI, are publicly available through National Aeronautics and Space Administration (NASA) Earthdata. ERA5 hourly 10 m winds are available from the Copernicus Climate Data Store (Hersbach et al., 2020). The breakpoint-regression formulation, the candidate-grid search, the acceptance criteria, the AR(1)-corrected acceptance rule, the product-specific native-pixel sampling rules, and the mesh construction are stated in full in Methods Sections 2.1–2.3 and Text S1 in the Supplement. The review-copy analysis archive accompanying this submission contains processing scripts, UC-window definitions, breakpoint-output parquet files, AR(1)-corrected derived tables, figure scripts, and manuscript table components in the `uidx/paperA` sub-project of https://github.com/ajsmit/ucxd. Before final submission, this repository snapshot and derived analysis tables will be archived in a FAIR-aligned (Findable, Accessible, Interoperable, Reusable) repository that assigns a digital object identifier (DOI), and that DOI should be cited here and in the reference list.

https://doi.org/10.5194/egusphere-2026-3017
Preprint. Discussion started: 23 June 2026

Author contributions. AJS designed the analysis, wrote the code, processed the data, produced the figures and tables, and wrote the first manuscript draft. NS contributed to the conceptual framing, Benguela interpretation, funding acquisition, and manuscript revision. Both authors reviewed and approved the submitted manuscript.

Competing interests. The authors declare that they have no competing interests.

Acknowledgements. This research was conducted under the financial support of the National Research Foundation (NRF) of South Africa: Effect of Coastal Ocean Extremes (ECOE), ESS240501216867. We thank the data providers whose operational products this work depends on: the Group for High Resolution Sea Surface Temperature (GHRSST) for the Level-4 SST analyses (the UK Met Office, the NOAA Office of Satellite and Product Operations, the NOAA National Centers for Environmental Information, and Remote Sensing Systems); the European Centre for Medium-Range Weather Forecasts (ECMWF) and the Copernicus Climate Change Service for ERA5; and Lamont et al. (2018) for the operational wind-phenology framework reused here.

Generative artificial intelligence (AI; Anthropic Claude Opus 4.7 Max) was used to manage and orchestrate the complex suite of R and Python scripts underpinning this analysis, including organising the operating environment and associated working directories, documenting scripts extensively, refactoring and optimising code, implementing parallel-processing workflows, and batch processing across multiple SST product lines. AI was also used to produce tables and figures in a manner that integrated these outputs seamlessly within the LaTeX documents, namely the main manuscript and supplementary materials, and to provide a final editorial pass for grammar and syntax prior to manuscript submission.

https://doi.org/10.5194/egusphere-2026-3017
Preprint. Discussion started: 23 June 2026

References

Abrahams, A., Schlegel, R., and Smit, A.: Variation and Change of Upwelling Dynamics Detected in the World's Eastern Boundary Upwelling Systems, Frontiers in Marine Science, 8, 2021a.

Abrahams, A., Schlegel, R. W., and Smit, A. J.: A novel approach to quantify metrics of upwelling intensity, frequency and duration, PLOS ONE, 16, https://doi.org/10.1371/journal.pone.0254026, 2021b.

Bai, J. and Perron, P.: Estimating and testing linear models with multiple structural changes, Econometrica, 66, 47–78, https://doi.org/10.2307/2998540, 1998.

Bakun, A.: Coastal Upwelling Indices, West Coast of North America, 1946–71, NOAA Technical Report NMFS SSRF-671, U.S. Department of Commerce, NOAA, National Marine Fisheries Service, Seattle, Washington, 1973.

Banzon, V., Smith, T. M., Chin, T. M., Liu, C., and Hankins, W.: A long-term record of blended satellite and in situ sea-surface temperature for climate monitoring, modeling and environmental studies, Earth System Science Data, 8, 165–176, 2016.

Belmajdoub, H., Minaoui, K., El Aouni, A., and El Abidi, Z.: Monitoring upwelling regions in major coastal zones using deep learning and sea surface temperature images, International Journal of Remote Sensing, 45, 4553–4575, 2024.

Belonenko, T. V., Budyansky, M. V., Akhtyamova, A. F., and Udalov, A. A.: Investigation of the Benguela upwelling eddies using Lagrangian modeling methods, Ocean Dynamics, 74, 373–390, 2024.

Benazzouz, A., Pelegrí, J. L., Demarcq, H., Machín, F., Mason, E., Orbi, A., Peña-Izquierdo, J., and Soumia, M.: On the temporal memory of coastal upwelling off NW Africa, Journal of Geophysical Research: Oceans, 119, 6356–6380, 2014a.

Benazzouz, A., Soumia, M., Abdellatif, O., Mohamed, C., Karim, H., Abderrahman, A., Pelegrí Josep, L., and Hervé, D.: An improved coastal upwelling index from sea surface temperature using satellite-based approach: the case of the Canary Current upwelling system, Continental Shelf Research, 81, 38–54, https://doi.org/10.1016/j.csr.2014.03.012, 2014b.

Bograd, S. J., Schroeder, I., Sarkar, N., Qiu, X., Sydeman, W. J., and Schwing, F. B.: Phenology of coastal upwelling in the California Current, Geophysical Research Letters, 36, L01 602, https://doi.org/10.1029/2008GL035933, 2009.

Bordbar, M. H., Mohrholz, V., and Schmidt, M.: The relation of wind-driven coastal and offshore upwelling in the Benguela Upwelling System, Journal of Physical Oceanography, 51, 3117–3133, 2021.

Brandt, P., Bordbar, M. H., Coelho, P., Koungue, R. A. I., Körner, M., Lamont, T., Lübbecke, J. F., Mohrholz, V., Prigent, A., Roch, M., et al.: Physical drivers of Southwest African coastal upwelling and its response to climate variability and change, in: Sustainability of southern African ecosystems under global change: Science for management and policy interventions, pp. 221–257, Springer, 2024.

Burnham, K. P. and Anderson, D. R.: Multimodel inference: understanding AIC and BIC in model selection, Sociological methods & research, 33, 261–304, 2004.

Byrt, T., Bishop, J., and Carlin, J. B.: Bias, prevalence and kappa, Journal of Clinical Epidemiology, 46, 423–429, https://doi.org/10.1016/0895-4356(93)90018-V, 1993.

Chelton, D. B.: Effects of sampling errors in statistical estimation, Deep-Sea Research Part A, 30, 1083–1103, https://doi.org/10.1016/0198-0149(83)90062-6, 1983.

Chen, Z., Yan, X.-H., Jo, Y.-H., Jiang, L., and Jiang, Y.: A study of Benguela upwelling system using different upwelling indices derived from remotely sensed data, Continental shelf research, 45, 27–33, 2012.

Chicco, D. and Jurman, G.: The advantages of the Matthews correlation coefficient (MCC) over F1 score and accuracy in binary classification evaluation, BMC Genomics, 21, 6, https://doi.org/10.1186/s12864-019-6413-7, 2020.

https://doi.org/10.5194/egusphere-2026-3017
Preprint. Discussion started: 23 June 2026

Hagen, E., Feistel, R., Agenbag, J. J., and Ohde, T.: Seasonal and interannual changes in intense Benguela upwelling (1982–1999), Oceanologica Acta, 24, 557–568, 2001.

Hersbach, H., Bell, B., Berrisford, P., Hirahara, S., Horányi, A., Muñoz-Sabater, J., Nicolas, J., Peubey, C., Radu, R., Schepers, D., Simmons, A., Soci, C., Abdalla, S., Abellan, X., Balsamo, G., Bechtold, P., Biavati, G., Bidlot, J., Bonavita, M., De Chiara, G., Dahlgren, P., Dee, D., Diamantakis, M., Dragani, R., Flemming, J., Forbes, R., Fuentes, M., Geer, A., Haimberger, L., Healy, S., Hogan, R. J., Hólm, E., Janisková, M., Keeley, S., Laloyaux, P., Lopez, P., Lupu, C., Radnoti, G., de Rosnay, P., Rozum, I., Vamborg, F., Villaume, S., and Thépaut, J.-N.: The ERA5 global reanalysis, Quarterly Journal of the Royal Meteorological Society, 146, 1999–2049, https://doi.org/10.1002/qj.3803, 2020.

Hurvich, C. M. and Tsai, C.-L.: Regression and time series model selection in small samples, Biometrika, 76, 297–307, https://doi.org/10.1093/biomet/76.2.297, 1989.

Hutchings, L., van der Lingen, C. D., Shannon, L. J., Crawford, R. J. M., Verheye, H. M. S., Bartholomae, C. H., van der Plas, A. K., Louw, D., Kreiner, A., Ostrowski, M., Fidel, Q., Barlow, R. G., Lamont, T., Coetzee, J., Shillington, F., Veitch, J., Currie, J. C., and Monteiro, P. M. S.: The Benguela current: An ecosystem of four components, in: Progress in Oceanography, vol. 83, pp. 15–32, Elsevier, https://doi.org/10.1016/j.pocean.2009.07.046, 2009.

Iles, A. C., Gouhier, T. C., Menge, B. A., Stewart, J. S., Haupt, A. J., and Lynch, M. C.: Climate-driven trends and ecological implications of event-scale upwelling in the California Current System, Global Change Biology, 18, 783–796, https://doi.org/10.1111/j.1365-2486.2011.02567.x, 2012.

Kämpf, J. and Chapman, P.: The Benguela Current upwelling system, in: Upwelling Systems of the World: A Scientific Journey to the Most Productive Marine Ecosystems, pp. 251–314, Springer, 2016.

Lamont, T., Hutchings, L., van den Berg, M. A., Goschen, W. S., and Barlow, R. G.: Hydrographic variability in the St. Helena Bay region of the southern Benguela ecosystem, Journal of Geophysical Research: Oceans, 120, 2920–2944, https://doi.org/10.1002/2014JC010619, 2015.

Lamont, T., García-Reyes, M., Bograd, S., Van Der Lingen, C., and Sydeman, W.: Upwelling indices for comparative ecosystem studies: Variability in the Benguela Upwelling System, Journal of Marine Systems, 188, 3–16, 2018.

Lutjeharms, J. and Meeuwis, J.: The extent and variability of South-East Atlantic upwelling, South African Journal of Marine Science, 5, 51–62, https://doi.org/10.2989/025776187784522621, 1987.

Lutjeharms, J. and Valentine, H.: Water types and volumetric considerations of the South-East Atlantic upwelling regime, South African Journal of Marine Science, 5, 63–71, 1987.

Marcello, J., Hernandez-Guerra, A., Eugenio, F., and Fonte, A.: Seasonal and temporal study of the northwest African upwelling system, International Journal of Remote Sensing, 32, 1843–1859, https://doi.org/10.1080/01431161003631576, 2011.

Matthews, B. W.: Comparison of the predicted and observed secondary structure of T4 phage lysozyme, Biochimica et Biophysica Acta – Protein Structure, 405, 442–451, https://doi.org/10.1016/0005-2795(75)90109-9, 1975.

Maturi, E., Harris, A., Mittaz, J., Sapper, J., Wick, G., Zhu, X., Dash, P., and Koner, P.: A new high-resolution sea surface temperature blended analysis, Bulletin of the American Meteorological Society, 98, 1015–1026, 2017.

Nykjaer, L. and Van Camp, L.: Seasonal and interannual variability of coastal upwelling along northwest Africa and Portugal from 1981 to 1991, Journal of Geophysical Research: Oceans, 99, 14 197–14 207, https://doi.org/10.1029/94JC00814, 1994.

https://doi.org/10.5194/egusphere-2026-3017
Preprint. Discussion started: 23 June 2026

Pavlushin, V. A. and Kubryakov, A. A.: Variability of the area and shape of the Benguela upwelling in 1985–2017 and its relation with dynamic characteristics from satellite measurements, Izvestiya, Atmospheric and Oceanic Physics, 58, 1037–1048, https://doi.org/10.1134/S0001433822090183, 2022.

Santos, A., Kazmin, A., and Peliz, A.: Decadal changes in the Canary upwelling system as revealed by satellite observations: their impact on productivity, Journal of Marine Research, 63, 359–379, 2005.

Schwarz, G.: Estimating the dimension of a model, The Annals of Statistics, 6, 461–464, https://doi.org/10.1214/aos/1176344136, 1978.

Seabra, R., Varela, R., Santos, A. M., Gomez-Gesteira, M., Meneghesso, C., Wethey, D. S., et al.: Reduced nearshore warming associated with Eastern Boundary Upwelling Systems, Frontiers in Marine Science, 6, https://doi.org/10.3389/fmars.2019.00104, 2019.

Vasquez-Cuervo, J., Dewitte, B., Chin, T. M., Armstrong, E. M., Purca, S., and Alburqueque, E.: An analysis of SST gradients off the Peruvian coast: the impact of going to higher resolution, Remote Sensing of Environment, 131, 76–84, https://doi.org/10.1016/j.rse.2012.12.010, 2013.

Wentz, F. J. and Meissner, T.: AMSR ocean algorithm, algorithm theoretical basis document, Remote Sensing Systems, 59, 2000.

Worsfold, M., Good, S., Atkinson, C., and Embury, O.: Presenting a long-term, reprocessed dataset of global sea surface temperature produced using the OSTIA system, Remote Sensing, 16, 3358, https://doi.org/10.3390/rs16183358, 2024.

Yao, Y.-C.: Estimating the number of change-points via Schwarz' criterion, Statistics & Probability Letters, 6, 181–189, https://doi.org/10.1016/0167-7152(88)90118-6, 1988.

Zhang, N. R. and Siegmund, D. O.: A modified Bayes information criterion with applications to the analysis of comparative genomic hybridization data, Biometrics, 63, 22–32, https://doi.org/10.1111/j.1541-0420.2006.00662.x, 2007.